Experimental and theoretical study of line mixing in methane spectra. II. Influence of the collision partner (He and Ar) in the v3 IR band

D. Pieroni, Nguyen-Van-Thanh, C. Brodbeck, J.-M. Hartmann, T. Gabard et al.

Citation: J. Chem. Phys. **111**, 6850 (1999); doi: 10.1063/1.480095
View online: http://dx.doi.org/10.1063/1.480095
View Table of Contents: http://jcp.aip.org/resource/1/JCPSA6/v111/i15
Published by the AIP Publishing LLC.

Experimental and theoretical study of line mixing in methane spectra. II. Influence of the collision partner (He and Ar) in the ν_3 IR band

D. Pieroni, Nguyen-Van-Thanh, C. Brodbeck, and J.-M. Hartmann[a)]
Laboratoire de Photophysique Moléculaire, UPR 3361 du CNRS, Université Paris Sud, Bâtiment 350, 91405 Orsay Cedex, France

T. Gabard and J.-P. Champion
Laboratoire de Physique de l'Université de Bourgogne, Unité Associée au CNRS, 9 Avenue Alain Savary, B. P. 47870, 21078 Dijon Cedex, France

D. Bermejo and J.-L. Domenech
Instituto de Estructura de la Materia, Consejo Superior de Investigaciones Cientificas, Serrano 123, 28006 Madrid, Spain

C. Claveau and A. Valentin
Laboratoire de Physique Moléculaire et Applications, UPR 136 du CNRS, Université Pierre et Marie Curie (T13), 4 Place Jussieu, 75252 Paris Cedex 05, France

M. V. Tonkov,[b)] I. M. Grigoriev,[b)] and R. Le Doucen
Laboratoire de Physique des Atomes, Lasers, Molécules, et Surfaces, Unité Mixte de Recherche du CNRS, Université de Rennes I, Campus de Beaulieu, 35042 Rennes Cedex, France

(Received 24 May 1999; accepted 27 July 1999)

Line mixing effects are studied in the ν_3 band of CH_4 perturbed by Ar and He at room temperature. Experiments have been made in the 2800–3200 cm^{-1} spectral region using four different setups. They cover a wide range of total densities, including low (0.25–2 atm), medium (25–100 atm), and high (200–1000 atm) pressure conditions. Analysis of the spectra demonstrates that the spectral shapes (of the band, the *Q* branch, the *P* and *R* manifolds,...) are significantly influenced by line mixing. The theoretical approach proposed in the preceding paper is used in order to model and analyze these effects. As done previously, semiclassical state-to-state rates are used together with a few empirical constants. Comparisons between measurements and spectra computed with and without the inclusion of line mixing are made. They prove the quality of the approach which satisfactorily accounts for the effects of pressure and of rotational quantum numbers on the spectral shape. It is shown that collisions with He and Ar lead to different line-coupling schemes (e.g., more coupling within the branches and less between branches) and hence to different shapes. The influence of line coupling between different branches and manifolds is evidenced and studied using high pressure spectra and absorption in the band wings. © *1999 American Institute of Physics.* [S0021-9606(99)01039-9]

I. INTRODUCTION

The influence of line mixing effects on infrared spectra of methane has been demonstrated in a number of recent papers.[1–5] These studies have shown that, when the absorption shapes are governed by collisions, the profiles of most spectral features (*Q* branch, *P* and *R* manifolds, clusters of lines) are significantly narrower than predicted when using purely Lorentzian line shapes. Two types of approaches, different in their principles, have been proposed in order to model line mixing and to correct for deviations from the isolated line approximation. The first, which is strictly empirical, was used in Refs. 1–3. Parameters representing line coupling are then determined (one by one) from fits of measured spectra. Very satisfactory agreement with experiments is obtained, but predictions are limited to (spectral, pressure) regions which have been investigated experimentally. A second type of approach was proposed in our previous paper[4] (referred to hereafter as PPI) which has more theoretical basis and requires much fewer empirical parameters. In this model, the off-diagonal elements of the relaxation matrix, which account for line coupling, are constructed starting from state-to-state rotational transfer rates. The latter are computed from the intermolecular potential by using a semiclassical model.[6,7] Connection between state-to-state data and the line coupling coefficients is made by introducing a few empirical parameters whose values are determined by fits of measured spectra. Comparisons of computed results with laboratory measurements of CH_4–N_2 absorption in the ν_3 band at room temperature between 0.5 and 50 atm have demonstrated[4] the predictive capability of the model. In a recent work, an approach similar to ours has been used by Pine *et al.*[5] for a refined study of both speed dependent and line mixing effects in low pressure methane spectra.

The present paper completes the study made in PPI by

a)Electronic mail: jean-michel.hartmann@ppm.u-psud.fr
b)Permanent address: Institute of Physics, St. Petersburg University, Peterhof 198904 St. Petersburg, Russia.

extending the pressure range investigated (up to about 1000 atm) and considering collisions with He and Ar. Measurements have been made using various setups of spectral resolutions adapted to the investigated densities. Analysis of the results show that the two collision partners considered induce different line mixing effects. The methane–helium interaction favors mixing within branches whereas interferences that occur between the *P*, *Q*, and *R* components are less important than for CH_4–Ar. Extension of the pressure range enables the study of the effects of coupling between different manifolds and branches on the central part as well as in the wings of the band. It is shown that our approach leads to satisfactory results over a very wide range of conditions.

The remainder of the article is organized in four sections. The theoretical model is recalled in Sec. II. The measured spectra and the data used for computations are described in Sec. III. Illustrative and representative comparisons between measured and computed spectra are presented in Sec. IV for a variety of total pressures. Specific problems, including the influence of the collision partner and the effects of intra- and interbranch mixings are discussed in Sec. V.

II. THEORETICAL MODEL

Since most theoretical elements have been described in PPI, only the main steps are recalled here.

For a CH_4–X mixture with densities n_{CH_4} and n_X ($n_{CH_4} \ll n_X$) at temperature *T*, the absorption coefficient α, accounting for line mixing at wave number σ is given by:

$$\alpha^{LM}(\sigma, n_{CH_4}, n_X, T) = \frac{8\pi^2\sigma}{3hc}[1-\exp(-hc\sigma/k_BT)] \times n_{CH_4}\,\mathrm{Im}\left\{\sum_k \sum_{k'} \rho_k(T) \times d_k d_{k'} \langle\langle k'|[\Sigma - \mathbf{L}_0 - i n_X \mathbf{W}_X(T)]^{-1}|k\rangle\rangle\right\}. \quad (1)$$

The sums include all absorption lines k and k', and ρ_k and d_k are, respectively, the initial level relative population and the dipole transition moment of line k. Σ, $\mathbf{L}_0$, and $\mathbf{W}_X$ are operators in the (Liouville) line space. The first two matrices are diagonal and real, associated with the scanning wave number σ and with the positions σ_k of the unperturbed lines. The relaxation operator $\mathbf{W}_X$ contains all the influence of collisions and depends on the band, on the temperature, and on the collision partner. Its off-diagonal elements account for interferences between absorption lines, whereas the diagonal terms are the pressure-broadening (γ_k) and shifting (δ_k) coefficients of the isolated lines [$\langle\langle k|\mathbf{W}|k\rangle\rangle = \gamma_k - i\,\delta_k$]. When line mixing is disregarded, the off-diagonal elements of $\mathbf{W}$ are neglected and Eq. (1) reduces to the addition of individual line contributions with Lorentzian shapes.

Recall that Eq. (1) assumes binary collisions and the impact approximation. Hence, $\mathbf{W}$ is independent on wave number and calculations must be restricted to the near wings of lines. Also note that refined effects, such as those related with velocity changes and speed averaging, are disregarded here. They have been studied in methane absorption at low pressures[2,5] but their influence is small under the conditions studied here (when compared with the precision of most our measurements and that of our model). Thus we have neglected them.

As in PPI, the imaginary off-diagonal elements of the relaxation operator are neglected and Im{$\mathbf{W}$} is restricted to its diagonal part (line shifts). The real part of the off-diagonal elements of $\mathbf{W}$ is constructed starting from state-to-state collisional rates and using some empirical factors in order to connect these data to the line coupling elements. The off-diagonal term coupling lines k and k' is then given by:

$$\mathrm{Re}\{\langle\langle k'|\mathbf{W}(T)|k\rangle\rangle\} = -A(k',k) \times K_{ik' \leftarrow ik}(T), \quad (k \neq k''), \quad (2)$$

where $K_{ik' \leftarrow ik}(T)$ is the collisional transfer rate from the lower level ik of line k to the lower level ik' of line k'. Simplifying hypotheses are made[4] in order to restrict the number of empirical parameters $A(k,k')$. The final approach used here is slightly different from that of PPI, for two reasons: the first is that the $A(R,R)$ and $A(P,P)$ parameters that govern coupling within manifolds may now depend on the rotational quantum number *J*. The second is that a specific factor $A(R,R') = A(P,P')$ is introduced for the intermanifold mixing in the *R* and *P* branches. The final parameters are then given by the following equations: for lines k and k' belonging to the same branch, the intrabranch parameters are given by:

$$\begin{aligned}
&k,k' \text{ are any } Q \text{ lines} \Rightarrow A(k',k) = A(Q,Q),\\
&k,k' \text{ are } R \text{ lines of the same } J \text{ manifold} \Rightarrow A(k',k) = A(R_J,R_J),\\
&k,k' \text{ are any } R \text{ lines of different manifolds} \Rightarrow A(k',k) = A(R,R'),\\
&k,k' \text{ are } P \text{ lines of the same } J \text{ manifold} \Rightarrow A(k',k) = A(P_J,P_J),\\
&k,k' \text{ are any } P \text{ lines of different manifolds} \Rightarrow A(k',k) = A(R,R'). \quad (3)
\end{aligned}$$

In order to further reduce the number of parameters and smooth the values obtained, we use a two-parameters modeling of the variations with rotational quantum number, i.e.,

$$A(R_{J-1},R_{J-1}) = A(P_J,P_J) = a + b \times J = a + b \times |m|. \quad (4)$$

Hence, as reasonably confirmed by the results of Sec. III B, we make the approximation that $A(R_{J-1},R_{J-1}) = A(P_J,P_J)$. The interbranch parameters are then determined in a second step by using the sum rule:[8]

$$\mathrm{Re}\{\langle\langle k|\mathbf{W}(T)|k\rangle\rangle\} = \gamma_k(T) = -\sum_{k' \neq k} \frac{d_{k'}}{d_k}\mathrm{Re}\{\langle\langle k'|\mathbf{W}(T)|k\rangle\rangle\}. \quad (5)$$

TABLE I. Groups and laboratory instruments involved in the measurements.

Group \ Characteristics	Instrument and resolution	He or Ar pressures (atm)	Regions
G1: LPPM-Orsay[a]	FT (Bruker IFS66V) 0.12 cm^{-1}	25, 50, 80, 100, 200, 300,..., 1000	P_{17} to R_{18}
G2: LPMA-Paris[a]	FT (home made) $\approx$0.01 cm^{-1}	2	P_{15} to R_{15}
G3: IEM-Madrid[a]	TDFS $\approx 10^{-4}$ cm^{-1}	0.25, 0.5, 1., 2.	R_J for J=8,10,12,14,16
G4: LPALMS-Rennes[b]	FT (Bruker IFS120) 0.002 cm^{-1}	0.25, 0.5, 1.	P_{12} to R_{19}

[a]See Ref. 4.
[b]See Ref. 9.

Indeed, in order to satisfy Eq. (5), the coupling between a given Q line, k, and all R and P lines, k', must be governed by the parameter $A(k',k)$ that only depends on k and is given by:

$$(k \in Q, k' \notin Q) \Leftrightarrow A(k',k) = \frac{\gamma_k - \Sigma_{k'' \in Q, k'' \neq k} d_{k''} \times A(k'',k) \times K_{ik'' \leftarrow ik}}{\Sigma_{k'' \notin Q} d_{k''} \times K_{ik'' \leftarrow ik}}. \quad (6)$$

Once these $R \leftarrow Q$ and $P \leftarrow Q$ terms are known, detailed balance gives the $Q \leftarrow R$ and $Q \leftarrow P$ couplings and only the $R \leftrightarrow P$ mixings remain unknown. The latter are then again derived from Eq. (5). The associated parameters $A(k',k)$ only depend on k and are given by:

$$\begin{pmatrix} k \in X = R \text{ or } P \\ k' \in Y = P \text{ or } R \end{pmatrix} \Leftrightarrow A(k',k) = \frac{\gamma_k - \Sigma_{k'' \in (Q \text{ or } X), k'' \neq k} d_{k''} \times A(k'',k) \times K_{ik'' \leftarrow ik}}{\Sigma_{k'' \in Y} d_{k''} \times K_{ik'' \leftarrow ik}}. \quad (7)$$

Note that the $R \leftarrow P$ and $P \leftarrow R$ couplings constructed this way insure that Eq. (5) is respected for P and R lines but do not rigorously verify detailed balance. An alternative way would be to construct $R \leftarrow P$ terms and deduce the $P \leftarrow R$ couplings from detailed balance but this would lead to the breakdown of Eq. (5) for R lines. A comparison between these two approaches has shown that they lead to very similar results for the conditions investigated here. Once the state-to-state rates and broadening coefficients are known, the model is thus based on four parameters only [$A(Q,Q)$, $A(R,R')$, and (a,b) in Eq. (4)]. They are empirical, depend on the collision partner, and need to be determined from fits of measured spectra as done in Sec. III B. Note that, in PPI, we assumed $A(R,R')=A(R,R)$; this approximation, which concerns the coupling between different manifolds within the P and R branches was a reasonable first guess. Its check requires pressures (not studied in PPI) high enough (above 200 atm) to make the manifolds overlap significantly. The present experiments at elevated density show that this approximation is not satisfactory and the $A(R,R')$ parameter has thus been introduced. Also note that Eqs. (6) and (7) define line dependent interbranch coupling factors that insure that the sum rule in Eq. (5) is rigorously respected. This was not the case in PPI where average interbranch factors were used.

The state-to-state rates $K_{ik' \leftarrow ik}(T)$ have been calculated from the CH_4–X interaction potential with a semiclassical model as described in Refs. 4, 6, 7.

III. DATA USED

A. Measured spectra

Absorption spectra have been measured in a wide pressure range (0.2–1000 atm), by using four different set ups as summarized in Table I. Since the experimental apparatuses and procedures have been described in detail in a number of previous publications (see references in Table I), details are not given here. Use of a large range of density conditions brings much information on collisional processes. Indeed, the recordings made at low (0.25–2 atm) pressures by high spectral resolution instruments enable analysis of the shape of the features within the manifolds. They are sensitive to the couplings that occur between the closely spaced lines only and hence depend on very few of the relaxation matrix elements. At intermediate densities (25–100) atm, all the features that compose a manifold merge into a unique structure but the manifolds are still discernible and practically do not mix with each other. Absorption is governed by all couplings within the manifolds but remains little dependent on interference between different manifolds and branches. Finally, at high pressure (>200 atm), the only smooth contours remaining are the P, Q, and R branches which tend to merge into a unique peak. The band shape is then sensitive to all possible couplings, including intermanifolds and interbranch interferences.

Note that, at elevated pressure, deviations from the perfect gas must be accounted for. This was done for Ar and He by using the data of Refs. 10, 11, and, in the following, the pressures P used are not those measured (P_{meas}) but those of the perfect gas for the same density. Hence $P = n(P_{\text{meas}},T) \times k_B \times T/1.013$ where n is the density of molecules under the experimental (P_{meas},T) conditions [e.g., P=475 atm for P_{meas}=600 atm of argon]. Densities d in amagat unit are then given by $d(\text{Am}) = P(\text{atm})*273/T$.

B. Data used for the computations

The spectroscopic parameters (σ_k, ρ_k, and d_k) of the isolated (CH_4) molecule have been taken from the 1996 version of the HITRAN database.[12]

Widths and shifts of lines other than those of the ν_3 band of $^{12}CH_4$ where obtained from the HITRAN data base values for air broadening corrected (for Ar and He) using constant factors derived from Ref. 13. For the ν_3 band transitions, the diagonal elements of **W** (half widths γ_k and shift δ_k of the lines) for CH_4–He and –Ar have been carefully (particularly γ_k) determined using a variety of sources as explained in Appendix A. The reason for that is that conclusions on the model quality are crucially dependent on the broadening data used as mentioned in PPI and demonstrated in Appendix B.

State-to-state rates have been computed for CH_4–He and CH_4–Ar collisions at room temperature as described in Refs. 4, 6, 7. The interaction is represented as a sum of atom–atom contributions with parameters that have been fitted on published potential surfaces. Those of Refs. 14 and 15 have been used for the methane–argon and methane–helium systems, respectively. These references and the calculated values of methane line broadening parameters[16,17] indicate that the quality of potential surface for CH_4–Ar is poorer than that for CH_4–He. This may explain some of the results obtained thereafter and calculations with a more accurate potential surface[18] would be of interest and are in progress.

Only the real part of the off-diagonal elements of **W** was considered and coupling was restricted to the ν_3 band of $^{12}CH_4$. The contributions of all the other lines ($^{13}CH_4$, hot, and combination bands, ...) were computed through the addition of Lorentzian (Voigt) profiles. This approximation has little consequences on computed results since absorption in the studied region is largely dominated by the contribution of the ν_3 band. The $\mathrm{Re}\{\langle\langle k'|\mathbf{W}(T)|k\rangle\rangle\}$ terms were calculated, up to $J=17$ ($\approx$400 lines) using the state-to-states rates and Eqs. (2)–(7). The needed values of a, b, $A(R,R')$, and $A(Q,Q)$ for the perturbers considered here have been determined as explained below.

The empirical constants of the model have been determined from least squares fit of measured absorption with the approach and data described above. The J dependent parameters $A(R_J,R_J)$ and $A(P_J,P_J)$ have first been retrieved by using both low (1 and 2 atm) and medium (25 atm) pressure spectra. Their values are plotted in Fig. 1 vs. m ($=J+1$ and $-J$ in the R and P branches, respectively). When significant, the results extracted in the P and R branches are consistent indicating that the use of the rotational quantum number m in Eq. (4) is reasonable. (As indicated by the error bars, some results have large uncertainties due to the small sensitivity of measured absorption to the considered parameter. It is the case of the values obtained from low pressure absorption in the P branch since lines within the P manifolds are to sparse to be significantly affected by line mixing at low pressures. It is also the case of the low J manifolds at medium pressures since their structures are then masked by the Q branch wings and almost indiscernible.) Furthermore, the values obtained from low and medium pressure spectra are in agreement (within uncertainties); possible explanations for the differences are discussed in Appendix B in terms of the influence of the half width data used. A fit of all values (accounting for uncertainties) was then made using Eq. (4) yielding the a and b parameters. Although quite crude, this procedure has a practical interest, and it enables ''smoothing'' of the results obtained for the various lines and pressures since errors on the broadening parameter for some specific transitions can affect the retrieved values of $A(m)$ (see Appendix B). Note that $A(J)$ parameters for R and P lines up to $J=10$ have been very carefully extracted by Pine *et al.*[5] from low pressure ($<$0.7 atm) spectra. The values obtained for CH_4–Ar are consistent (considering uncertainties) with our set derived from low pressure absorption but show a much smoother behavior probably due to the fact that widths and shifts are simultaneously fitted in Ref. 5. As in PPI, the value of $A(Q,Q)$ was determined from spectra at intermediate density. Finally, the $A(R,R')$ parameter was obtained from absorption at high pressure, all other parameters being fixed. The final set of constants is summarized in Table II.

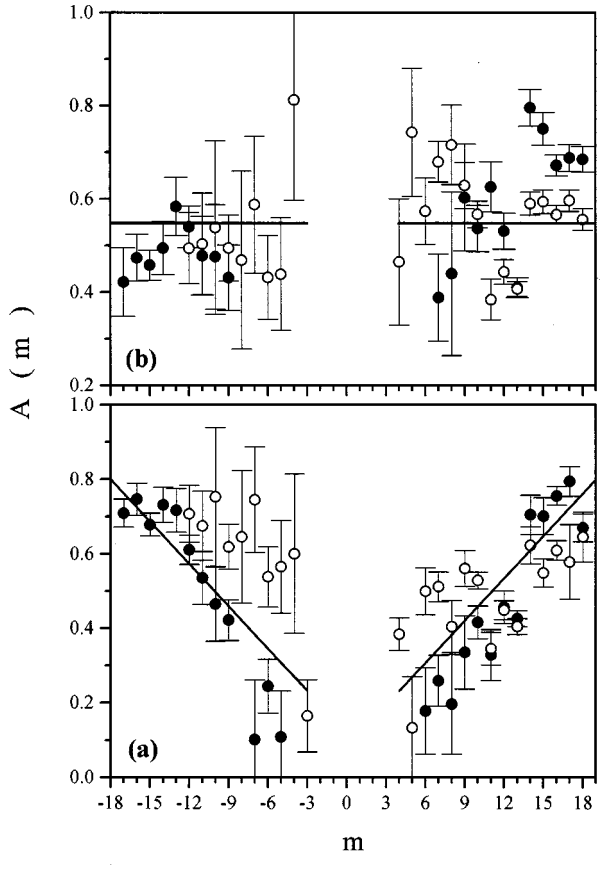

FIG. 1. Values of $A(m)$ [i.e., $A(R_J,R_J)$ and $A(P_J,P_J)$]. ● and ○ have been retrieved from low (groups G2–G4) and medium (group G1) pressure spectra, respectively. — are the fits using Eq. (4). (a) and (b) are for He and Ar.

TABLE II. $A(X,Y)$ parameters used in the present work.

	CH_4–He	CH_4–Ar
$A(Q,Q)$	0.450	0.282
$A(R,R)$	$0.081+0.038\lvert m\rvert$	0.547
$A(R,R')$	0.490	0.198

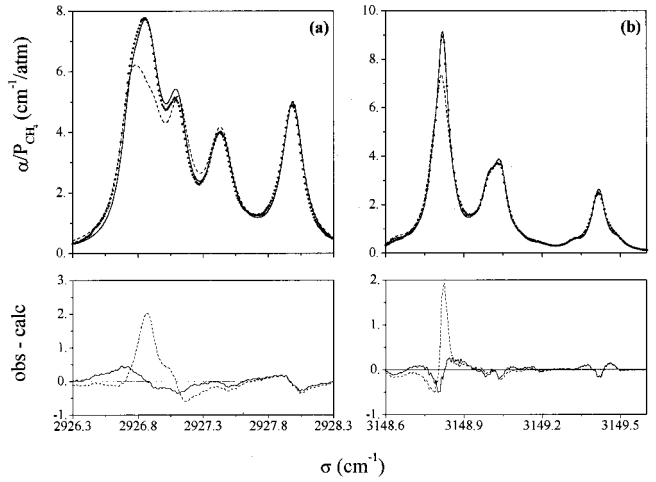

FIG. 2. Measured and calculated absorption in P and R manifold at low pressure. ● are measured values whereas — and --- have been calculated with and without the inclusion of line mixing, respectively. Obs–calc deviations are given in the lower part of the plot. (a) P_9 lines in CH_4–Ar under 2.00 atm (group G2). (b) R_{13} lines in CH_4–He under 0.987 atm (group G4).

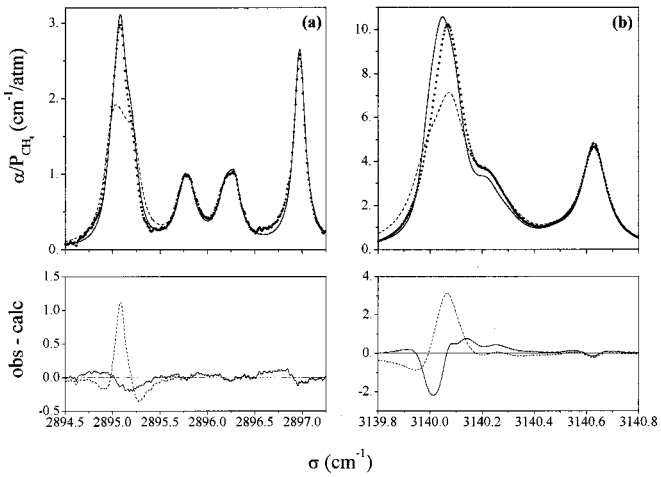

FIG. 3. Same as in Fig. 2 but for: (a) P_{12} lines in CH_4–Ar under 2.00 atm (group G2). (b) R_{12} lines in CH_4–He under 1.97 atm (group G4).

IV. RESULTS

This section is devoted to comparisons between measured and computed spectra in order to assess the quality of our approach. Effects of line mixing on low and medium pressure spectra have been discussed in the case of CH_4–N_2 in our previous paper. Since the behaviors observed for methane–argon and methane–helium mixtures are qualitatively similar to that of methane–nitrogen, only a brief de-

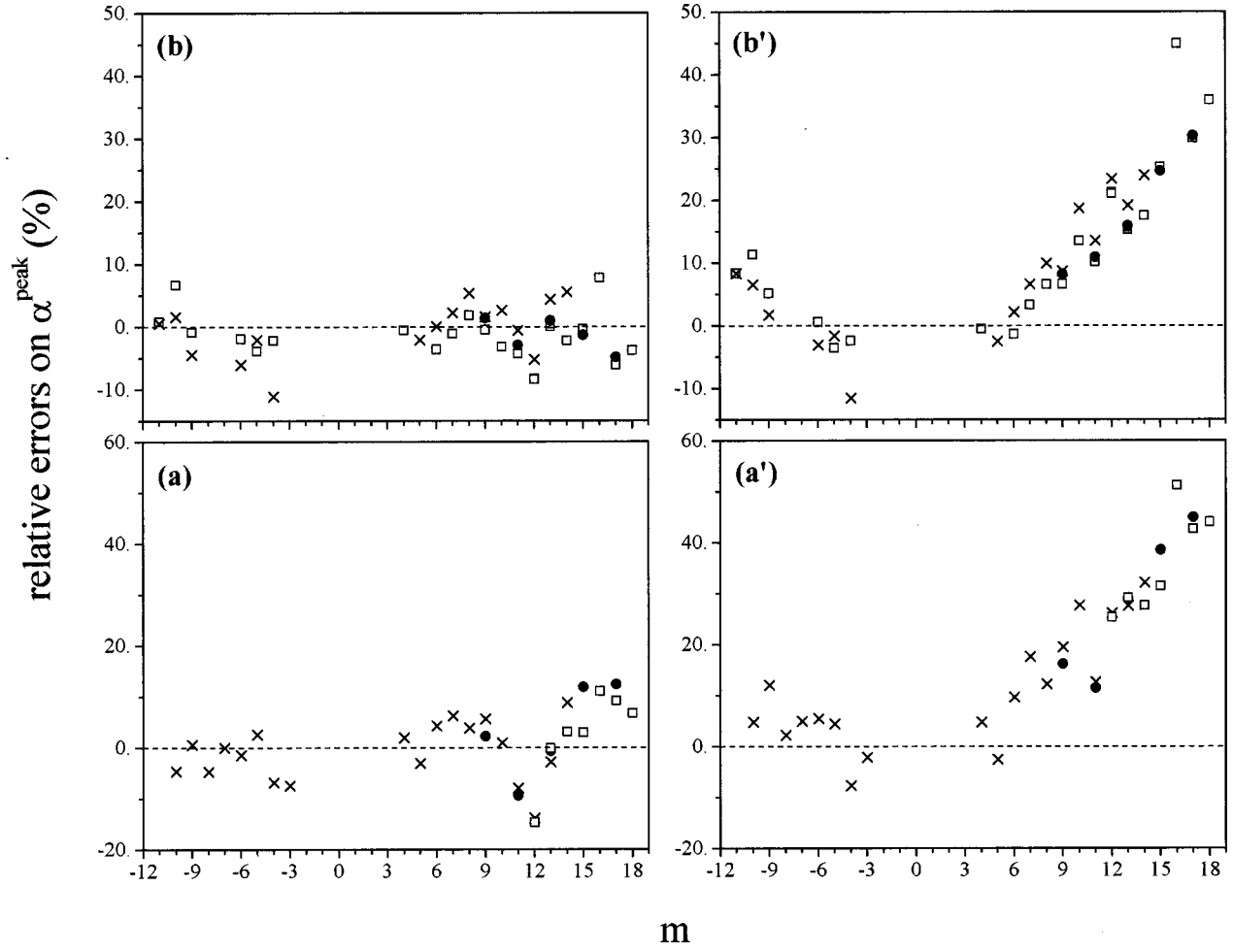

FIG. 4. Relative errors on the computed peak absorption of the ν_3 band features for a pressure of about 1 atm. Values in the R and P manifolds are plotted vs. rotational quantum number m. ×, ●, and □ are values deduced from measurements by groups G2, G3, and G4, respectively. (a) and (b) are results obtained with our model for Ar and He, respectively. (a′) and (b′) are the corresponding results obtained neglecting line mixing.

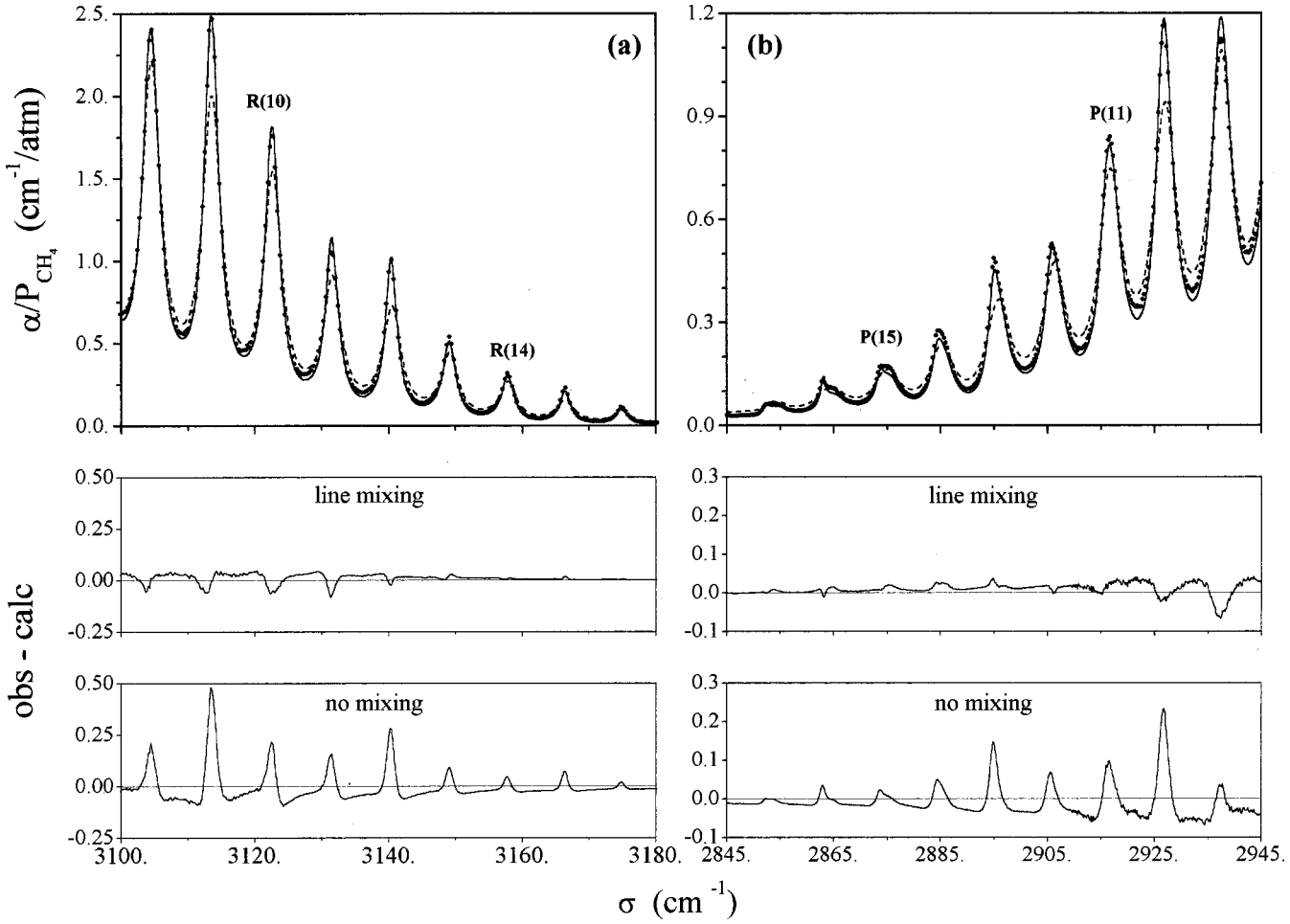

FIG. 5. Absorption in the R and P branches for the pressure of about 50 atm. ● are measured values (group G1) whereas — and --- have been calculated with and without the inclusion of line mixing, respectively. Obs−calc deviations are given in the lower part of the plot. (a) R_8−R_{16} for CH_4–He. (b) P_{17}−P_9 for CH_4–Ar.

scription of results is given here. A few representative spectra, recalling the main points are presented and more information (e.g., on the line structure) can be found in Ref. 4.

A. Low pressures (0.25–2 atm)

As shown in Refs. 4, 3, 5, detailed information on what happens inside the spectral structures is brought by low pressure absorption. Regions near the centers of P and R manifolds are considered here and results in the Q branch are not presented since the highest pressure studied (2 atm) is too low to induce large line mixing effects (they remain lower than a few %).

Figure 2 presents results obtained in the P_9 and R_{13} manifolds. The improvement obtained when modeling line mixing with our approach is clear. Furthermore, and as noted previously [Figs. 10(a), 11(a), and 11(b) of PPI], our model reproduces the high selectivity of collisional processes: it does correctly account for the fact that F_1 and F_2 components on the low frequency side mix, whereas those on the right hand side are practically unaffected. Measured and computed spectra in the P_{12} and R_{12} manifolds are plotted in Fig. 3. Line mixing has effects in the left hand side clusters only whereas lines on the high frequency side are uncoupled, as expected, since they are of different nuclear spin symmetries (A, E, and F). Note that the use of an improved line broadening data set (see Appendix A) has considerably improved the quality of predictions in this A,E,F cluster [compare Fig. 3(a) with Fig. 12(a) of PPI].

An overview of the quality of predictions is given by Fig. 4, where relative errors on the peak absorption of manifolds for a total pressure of ≈1 atm are plotted. These results demonstrate the consistency of the various experimental results. They show, for He and Ar, that neglecting line mixing leads to errors that increase with J and reach a factor of about two for high rotational quantum number lines.

B. Intermediate pressures (25–100 atm)

Figure 5 presents measured and calculated spectra in the P and R branches for a total pressure of about 50 atm. These plots, which confirm the quality of our approach, are very similar and call for the same conclusions as for CH_4–N_2 (Figs. 3 and 4 of PPI). The view of the entire band for CH_4–He in Fig. 6 is also equivalent to results for CH_4–N_2 (Fig. 5 of PPI). Again, line mixing has large effects in the Q branch and in the troughs between high J manifolds. Our approach leads to satisfactory results whereas neglecting line mixing strongly underestimates the Q branch peak and over-

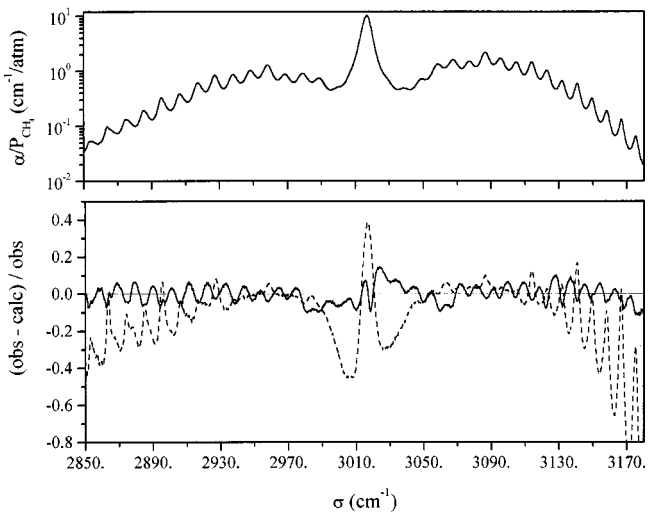

FIG. 6. Absorption in the whole band for the pressure 98.9 atm of He. Measured values (group G1) are plotted in the upper part. (obs–calc)/obs relative deviations are displayed in the lower part where — and --- have been calculated with and without the inclusion of line mixing, respectively.

estimates the far wings. In particular, as observed for CH_2–N_2 (Ref. 4) and some other molecular systems,[19] inclusion of line coupling significantly reduces absorption in the troughs between high rotational quantum number lines.

For a synthetic view of the effects of collisions, we have determined (as in PPI) the half width at half maximum $\Gamma(P_X)$ of each absorption feature (Q branch, R and P manifolds) in the 25 and 50 atm spectra for X=He and X=Ar. The results have then been fitted by the linear law:

$$\Gamma(P_X)=\Delta\sigma+P_X\times\gamma_X^{\mathrm{Eff}}. \tag{8}$$

The values of γ^{eff} deduced from measured and computed spectra are plotted in Fig. 7. The effective broadening coefficient of the manifold decreases with increasing J while the effects of line mixing become more and more important. When line coupling is neglected, errors reach about a factor of two as already indicated by the results at low pressure (Fig. 4). Although not perfect, our model accounts for most of the characteristics of the influence of rotational quantum numbers on the spectral shape at these intermediate pressures. Most errors on computed results are due to use of Eq. (4) instead of the original values (in Fig. 1) retrieved from spectra. Note that the broadening of the Q branch is significantly smaller for methane in helium than in argon; the situation is the same for the manifolds although differences vanish for high J lines. This point is discussed in the next section.

C. High pressures (200–800 atm)

Measured and calculated spectra at high pressures are shown in Figs. 8 and 9. Our approach leads to satisfactory results, whereas neglecting line mixing strongly overestimates the Q branch width and the absorption in the band wings. Note that, contrary to CH_4–He, all branches start to merge and the troughs between the Q and R,P branches tend to fill up in CH_4–Ar spectra at elevated pressure [Fig. 8(a)].

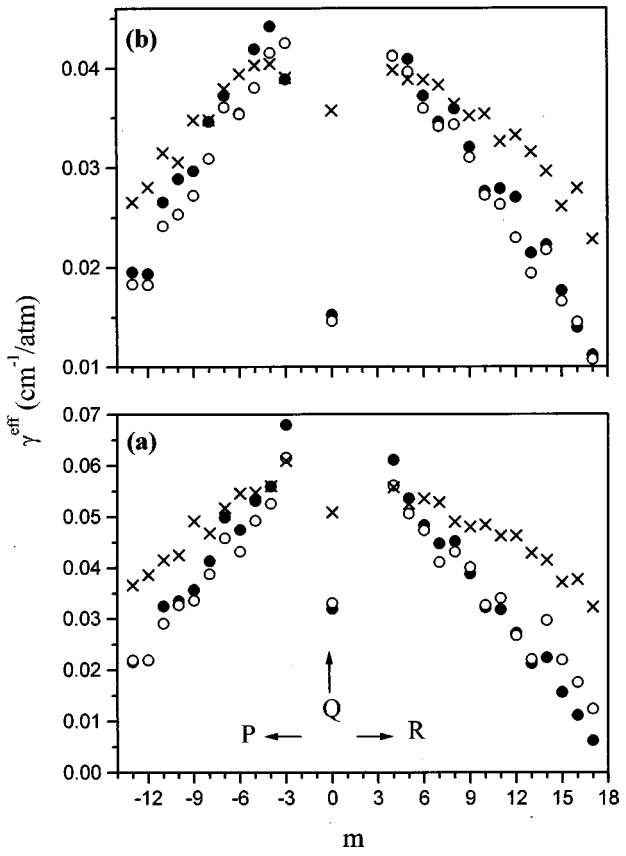

FIG. 7. Effective broadening coefficients γ^{eff} [see Eq. (8)] of the ν_3 band features. Values in the R and P manifolds are plotted vs. rotational quantum number m ($-J$ and $J+1$ for P and R lines, respectively) and the results for the Q branch are given at the position $m=0$. ● have been obtained from measured spectra (group G1); ○ and × were deduced from absorption calculated with and without the inclusion of line mixing, respectively. (a) is for Ar, (b) is for He.

This effect, which is similar to that observed in CO_2,[20,21] results from interbranch mixing and is analyzed in the following.

V. DISCUSSION ON SPECIFIC POINTS

This section is devoted to the discussion of the effects of the collision partner and of mixing between the various spectral components of the spectrum. For quantitative comparisons, we introduce some (intensity weighted) branch-averaged collisional quantities, that are given by the general expression:

$$\overline{C}_{X\leftrightarrow Y}=\mathrm{Re}\left[\sum_{\substack{k\in Y\\ k'\in X}}\rho_k d_k d_{k'}\times\langle\langle k'|\mathbf{W}|k\rangle\rangle+\sum_{\substack{k\in X\\ k'\in Y}}\rho_k d_k d_{k'}\times\langle\langle k'|\mathbf{W}|k\rangle\rangle\right]\Bigg/\left[\sum_{k\in X,Y}\rho_k\times d_k^2\right]. \tag{9}$$

We have calculated the values of the average intrabranch terms ($C_{P\leftrightarrow P}$, $C_{Q\leftrightarrow Q}$, and $C_{R\leftrightarrow R}$), and the mean interbranch couplings ($C_{Q\leftrightarrow P,R}$ and $C_{R\leftrightarrow P}$). The first three parameters govern the shape of isolated branches and are the associated branch broadening parameters. The others are responsible for

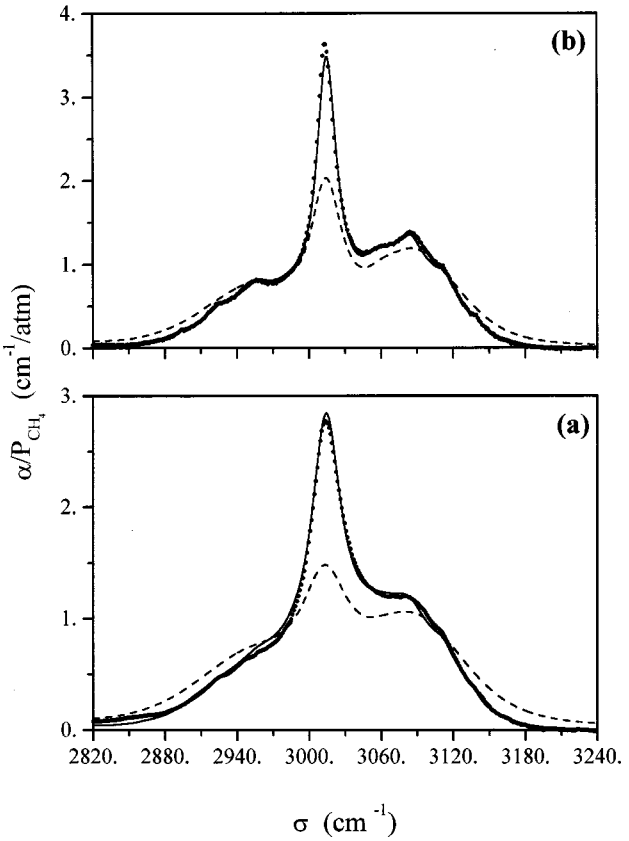

FIG. 8. Measured and calculated spectra for CH_4–Ar at high pressure. ● are measured values (group G1) whereas — and --- have been calculated with and without the inclusion of line mixing, respectively. (a) and (b) are for the total pressures 475 and 297 atm, respectively.

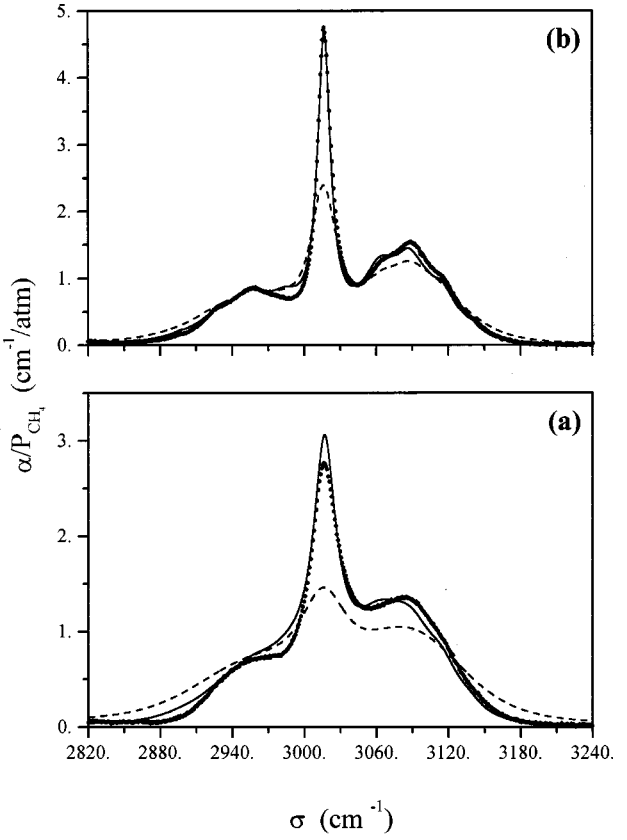

FIG. 9. Measured and calculated spectra for CH_4–He at high pressure. Same symbols as in Fig. 8. (a) and (b) are for the total pressures 692 and 337 atm, respectively.

the transfers between the *P*, *Q*, and *R* components. The values obtained, which are gathered in Table III, are used in the discussion below. The results obtained for $C_{X\leftrightarrow X}$ with and without the inclusion of line mixing (left and right parts of Table III) demonstrate the narrowing of branches due to coupling.

A. Effect of the perturber

In order to compare the effects of collisions with He and Ar on the spectral shape, two different approaches can be used. In the first, the (real) pressure *P* is used as a parameter, as was done in Fig. 7. In this case, CH_4–He collisions lead to narrower profiles than those induced by the CH_4–Ar interaction for all structures (*Q* branch and the *P* and *R* manifolds). In these ''absolute'' comparisons, not only line mixing effects through the off diagonal elements of **W**, but also the line broadening (diagonal terms) make a contribution. The fact that the widths of lines are different for CH_4–He and –Ar collisions makes the evaluation of the relative contributions of line mixing difficult when the true pressure is used. For ''relative'' comparisons, we introduce the ''equivalent pressure'' P_{eq} that makes line broadening for He and Ar similar. The helium is used as a reference [i.e., $P_{eq}(\mathrm{He}) = P(\mathrm{He})$] and the values for argon are given by:

$$P_{eq}(\mathrm{Ar}) = P(\mathrm{Ar}) \times [\gamma_{\mathrm{Ar}}/\gamma_{\mathrm{He}}]^{\mathrm{Av}}, \tag{10}$$

where $[\gamma_{\mathrm{Ar}}/\gamma_{\mathrm{He}}]^{\mathrm{Av}}$ is the line averaged ratio of Ar to He line broadening parameters of methane lines [its value at room temperature is 1.39.][13] Since the line-to-line variations of $\gamma_{\mathrm{Ar}}/\gamma_{\mathrm{He}}$ are moderate,[13] CH_4–He and CH_4–Ar spectra computed without inclusion of line mixing (diagonal relaxation operator) for the same P_{eq} are almost identical (this is confirmed by the fact that values between parentheses in the right part of Table III are the same for Ar and He). Comparison of the relative effects of line coupling (off-diagonal elements) is then possible.

1. Low pressures

Peak absorption in some R_J manifolds at low density are plotted versus equivalent pressure in Fig. 10. As observed previously,[2,4,5] coupling between lines induces effects that increase with the number of collisions. Comparison of experimental results for CH_4–Ar and CH_4–He indicates that, for given P_{eq}, the profiles are narrower for Ar than for He, with a difference that increases with *J*. This shows that, with respect to the broadening, the off-diagonal elements of $\mathrm{Re}\{\mathbf{W}\}$ connecting lines of a given manifold are larger in the case of Ar, particularly for large rotational quantum numbers. Our model qualitatively reproduces the effect of the perturber and pressure but discrepancies remain, mostly due to use of $A(R_J, R_J)$ parameters smoothed by Eq. (4).

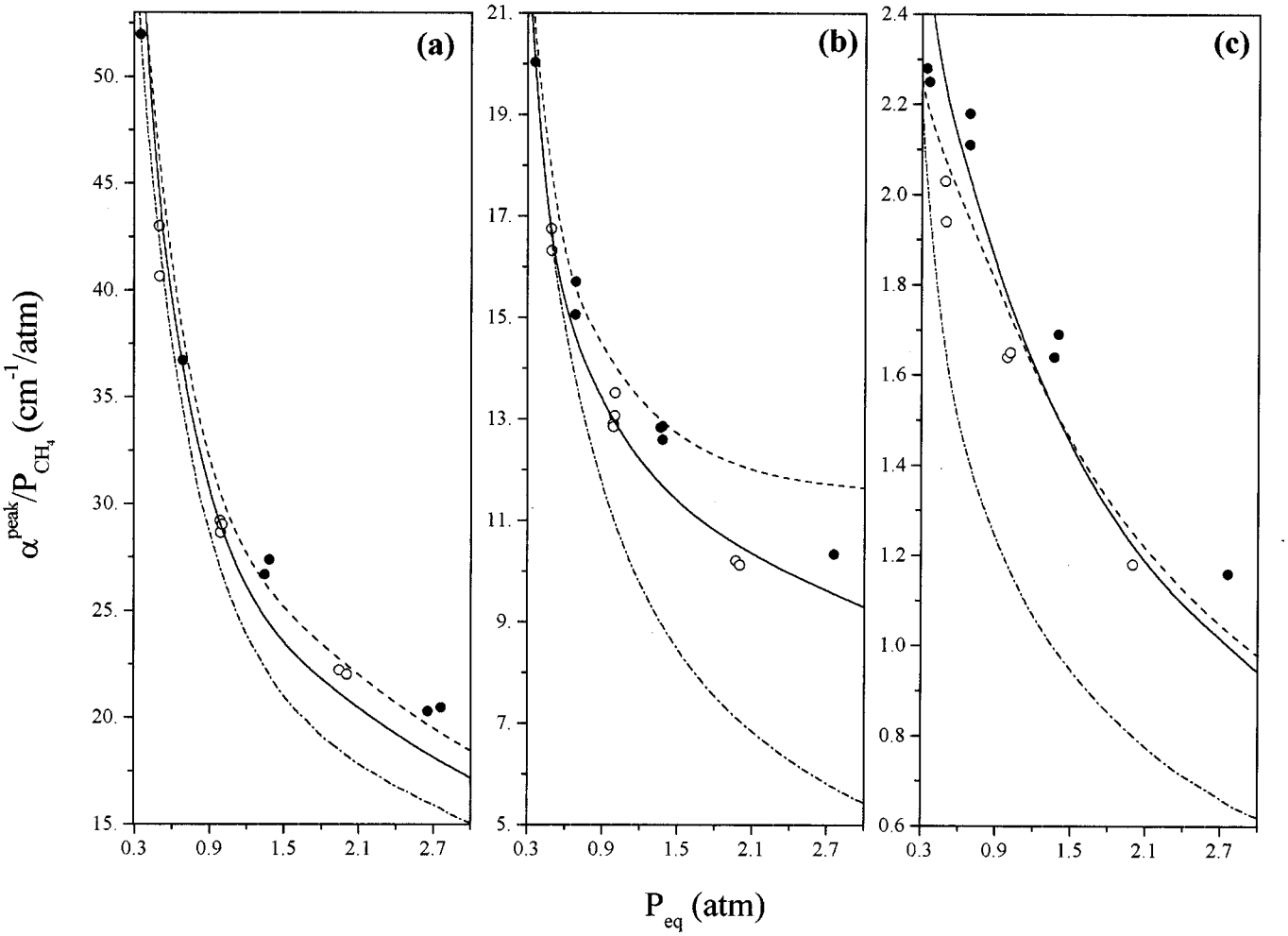

FIG. 10. Measured and calculated peak absorptions in R manifolds vs. equivalent pressure. ● and ○ are experimental results for Ar and He (groups G2, G3, G4), respectively. — and --- are the corresponding calculated values. The lower curve (— · —) was obtained neglecting line mixing (same results for He and Ar since P_{eq} is used). (a) (b), and (c) are for the R_8, R_{12}, and R_{16} manifolds, respectively.

2. Intermediate pressures

The spectra at intermediate density have been treated as in Sec. IV B in order to determine the widths of the spectral structures. The results were then fitted using Eq. (8) but now replacing P by P_{eq}. The values of the effective broadening parameters $\gamma^{\text{eff-eq}}$ per unit equivalent pressure are plotted in Fig. 11 for the P, Q, and R branches. They confirm the observation made at low pressure that the relative narrowing of P and R manifolds is more pronounced for Ar than for He, contrary to what is obtained when ''true'' pressure is used (Fig. 7). With respect to the broadening the coupling elements within a manifold are larger for Ar than for He (hence $\gamma^{\text{eff-eq}}(\text{Ar}) < \gamma^{\text{eff-eq}}(\text{He})$] but they remain too small to overcome the difference (factor 1.39) between the broadenings [hence $\gamma^{\text{eff}}(\text{Ar}) > \gamma^{\text{eff}}(\text{He})$]. Contrary to P and R manifolds, the Q branch is broader for CH_4–Ar mixtures than for the CH_4–He system showing that $Q-Q$ coupling elements are, with respect to the line broadening, more important for He. This result is consistent with the values of $C_{Q\leftrightarrow Q}$ given in Table III. A similar behavior has been observed for linear

TABLE III. Averages of the relaxation matrix elements (cm^{-1}/atm) as defined in Eq. (9). The values between parentheses are per unit equivalent pressure P_{eq} [Eq. (10)] whereas the others are per unit ''true'' pressure P.

	With line mixing		No line mixing	
	Ar	He	Ar	He
$C_{P\leftrightarrow P}$	0.035 (0.025)	0.019 (0.019)	0.052 (0.037)	0.037 (0.037)
$C_{Q\leftrightarrow Q}$	0.038 (0.027)	0.019 (0.019)	0.053 (0.038)	0.038 (0.038)
$C_{R\leftrightarrow R}$	0.032 (0.023)	0.017 (0.017)	0.052 (0.037)	0.037 (0.037)
$C_{Q\leftrightarrow R,P}$	−0.024 (−0.017)	−0.012 (−0.012)	0	0
$C_{R\leftrightarrow P}$	−0.016 (−0.011)	−0.008 (−0.008)	0	0

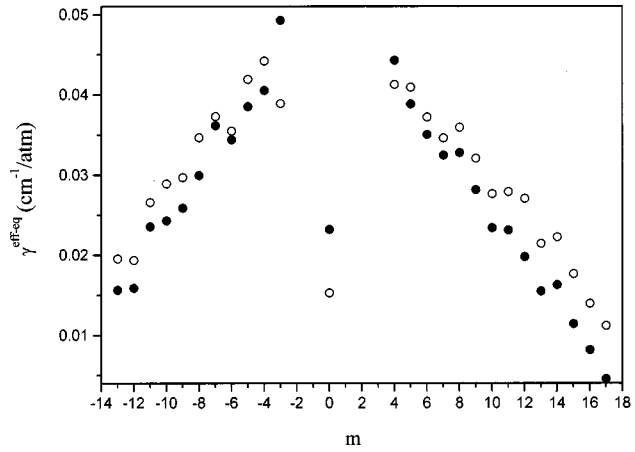

FIG. 11. Effective broadening coefficients $\gamma^{\text{eff-eq}}$ per unit equivalent pressure. Values in the R and P manifolds are plotted vs. rotational quantum number m ($-J$ and $J+1$ for P and R lines, respectively) and the results for the Q branch are given at the position $m=0$. ● and ○ are experimental results for Ar and He (group G1), respectively.

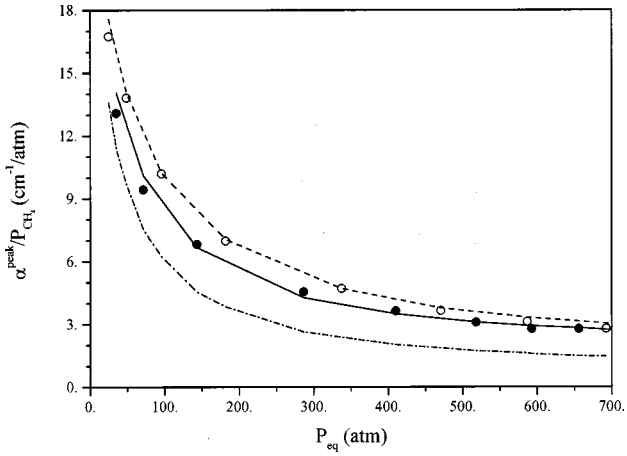

FIG. 13. Measured (group G1) and calculated absorptions at the Q branch peak vs. equivalent pressure. Same legend and symbols as in Fig. 10.

molecules which show significantly narrower Q branches when collisions with He are considered (e.g., Refs. 9, 22). This was explained in the case of CO_2 (Ref. 9) by the fact that the interaction potential is dominated by the repulsive front and mid- and long-range forces are much smaller than for other perturbers. Since the CH_4–He potential shows the same characteristic, the explanation given in Ref. 9 likely stands for methane.

3. High pressures

High density spectra of CH_4–Ar and CH_4–He for the same equivalent pressure are compared in Fig. 12. They confirm that the Q branch is broader in the case of collisions with Ar whereas the troughs between the branches is more pronounced for He. These differences can be explained looking at Table III: the broadening parameters ($C_{X\leftrightarrow X}$) of all branches are larger for Ar than for He when equivalent pressure is considered. Furthermore, interbranch mixings ($C_{X\leftrightarrow Y}$), which fill the troughs between the branches (see below) are also larger. Hence these two effects contribute to a less pronounced gap between the Q and P,R components. A synthetic comparison between absorptions at the Q branch peak is made in Fig. 13. Again, helium leads to higher peaks than Ar although the difference between perturbers vanishes with increasing pressure. This is due to the competitive effects of the broadening of the Q branch and of the contributions of the other branches. Indeed (see Table III), whereas for CH_4–Ar the Q branch is broader and thus has smaller peak absorption than for He, the larger broadenings of the P and R branches and of interbranch mixing make larger contributions at the band center.

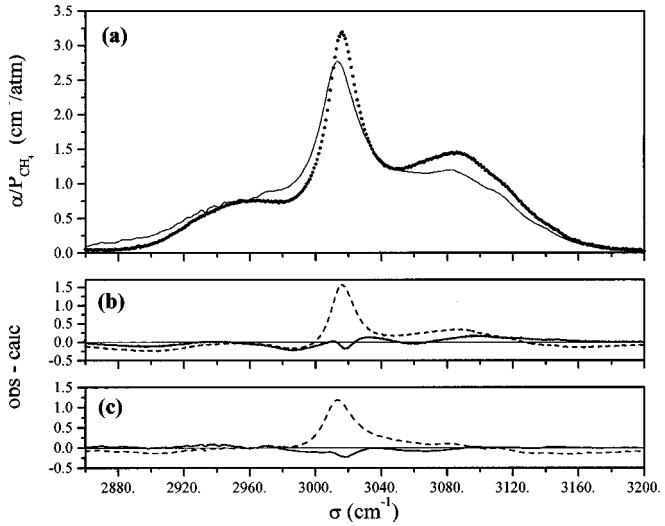

FIG. 12. Measured and calculated spectra for the equivalent pressure 589 atm. (a) Experimental values for He (●) and Ar (—) (group G1). (b) and (c) display the obs–calc deviations for He and Ar where — and --- have been calculated with and without the inclusion of line mixing.

B. Influence of intrabranch and interbranch mixing

As is well know from studies of other molecular systems (e.g., Refs. 23, 24) intrabranch mixings narrow the branches whereas interbranch couplings fill the troughs between branches. This is confirmed, in the case of CH_4–Ar by the results in Fig. 14 which should be read in the following way: starting from the purely Lorentzian calculation, we first introduce the intrabranch couplings. This leads to a narrowing of all branches (as indicated by the differences between values of $C_{X\leftrightarrow X}$ in the right and left part of Table III), hence to the enhancement of their peaks and the decrease of absorption between branches. Introducing $Q\leftrightarrow(R \text{ and } P)$ couplings takes intensity from the P and R wings and transfers it towards the $Q-R$ and $Q-P$ troughs. Finally, $R\leftrightarrow P$ mixings transfer intensity towards the central region of the band ($R-P$ trough) and lower the absorption at the R and P peaks and wings. The differences between He and Ar observed in Fig. 12 are then easily explained in view of Table III and of the preceding analysis: all C parameters being larger for argon, the overall profile is ''flatter'' with less marked branches than for helium since the branches are broader ($C_{X\leftrightarrow X}$) and the troughs are less deep ($C_{X\leftrightarrow Y}$).

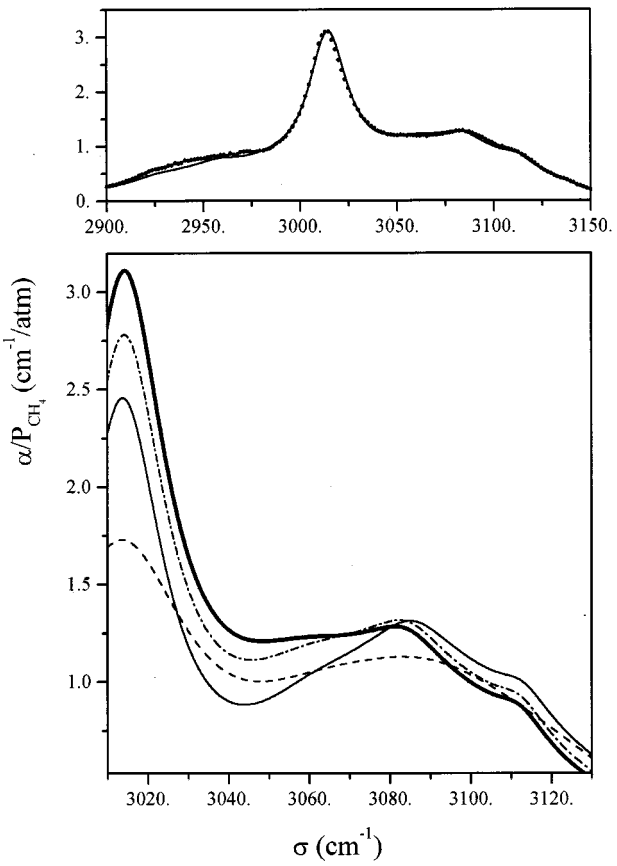

FIG. 14. Absorption for CH_4–Ar under the pressure 375 atm. The measured (group G1) and calculated spectra are displayed in the upper part. The lower part gives calculated values with the conventions: --- no line mixing (diagonal **W**), — diagonal and intrabranch terms ($R-R$, $Q-Q$, $P-P$), — · — diagonal, intrabranch terms, and $Q-P$ and $Q-R$ interbranch mixings, —— all terms ($P-P$, $Q-Q$, $R-R$, $Q-P$, $Q-R$, $R-P$).

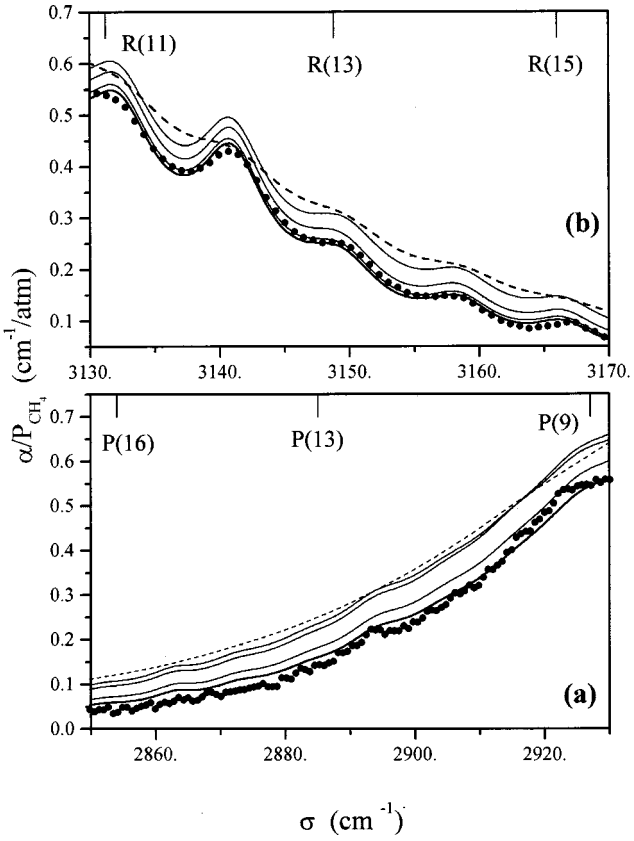

FIG. 15. Measured and calculated absorptions in the wings of the band. (a) The Ar broadened P branch wing for 297 atm. (b) The He broadened R branch wing for 181 atm. ● experimental results (group G1). --- are values calculated without line mixing. The — curves, starting from the top one and going down were obtained by successively introducing the mixings: within manifolds, between manifolds, between Q and (P,R) lines, and between R and P lines (full calculation).

C. Wing absorption

Correct modeling of spectra in the spectral regions of weak absorption is of crucial practical importance for atmospheric applications. In particular, these ''windows'' are used for the sounding of the deep parts of the atmospheres. The quality of our approach is demonstrated in Fig. 15 which also enables analysis of the various line coupling contributions. Starting from the Lorentzian (diagonal **W**) calculation we first introduce coupling within the manifolds. As widely demonstrated by the results of Sec. IV and obvious in Fig. 15(b), this leads to a sharpening of the shape of the manifolds. The introduction of intermanifold couplings then leads to a reduction of the absorption since intensity is transferred towards the more intense lines near the center of the P and R branches. Finally, the absorption is further lowered by interbranch mixings which transfer intensity to the central part of the band. A comparison of the effects of collisions with He and Ar on the wing absorption is shown in Fig. 16 where results obtained at the wavenumber between the $R13$ and $R14$ lines are presented. For both perturbers absorption is strongly subLorentzian, as has been observed for some other molecules with relatively narrow line spacing.[19,25] Note that this behavior is not systematic and that superLorentzian behaviors have been observed for some light molecules, likely due to finite duration of collision effects (e.g., Refs. 26, 27). At pressures below about 50 atm, the absorption in Fig. 16 results from wing contributions only and is a linear function of density. At elevated pressure the nearby lines start to overlap and make a contribution that decreases with density (at a line center, absorption is proportional to P^{-1}) and reduces

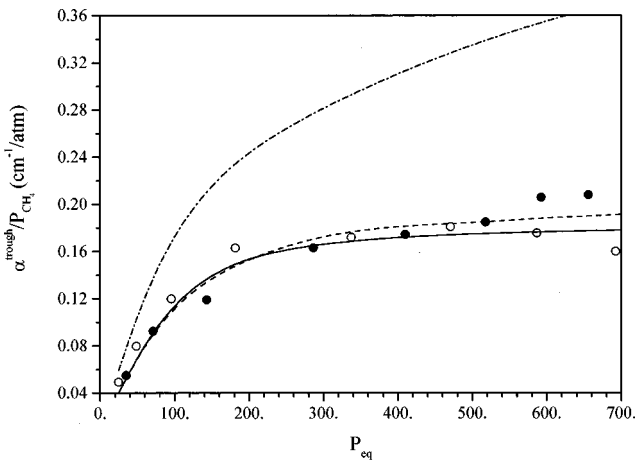

FIG. 16. Measured (group G1) and calculated absorptions at the wavenumber between the $R13$ and $R14$ lines vs. equivalent pressure. Same legend and symbols as in Fig. 10.

the increase of the overall absorption with pressure. Differences between results obtained for CH_4–He and CH_4–Ar are not clear, both experimentally and theoretically. Study of absorption in the further wing would be of interest.

Note that the quality of predictions obtained in the wing region may seem surprising since Eq. (1) is based on the impact approximation. Use of a relaxation operator independent on wave number should break down far away from the considered lines (e.g., Refs. 27–29). Indeed, this approximation is only valid for distances $\Delta\sigma$ lower than $(2\pi c\tau_c)^{-1}$ where τ_c is the typical duration of efficient collisions, i.e., typically of the order of 20 and 100 cm^{-1} for CH_4–Ar and –He collisions. The agreement between measured and calculated values in Figs. 15 and 16 is due to the fact that, in the regions considered, absorption is dominated by the contribution of the nearby manifolds.

VI. CONCLUSION

The model proposed in our previous paper has been applied to mixtures of methane with He and Ar. Comparisons between measured and computed spectra in a very wide range of pressures have demonstrated that line mixing effects are correctly accounted for by our approach. Differences between the collisional shapes induced by the two perturbers studied have been pointed out and analyzed. The influence of intermanifold and interbranch mixing has been evidenced by using high density absorption. Analysis of the results indicate that, when compared to CH_4–Ar, CH_4–He collisions favor intrabranch transfers to the detriment of interbranch couplings. The wing regions, which are of importance for atmospheric applications, has been studied showing that our model satisfactory predicts its strong subLorentzian behavior. Finally, the need for a large improvement of line broadening parameters in molecular spectroscopic databases has been demonstrated. Among the subjects of interest that remain unstudied are the influences of the band and of temperature on line mixing processes. These points are of crucial importance for applications since temperatures go down to about 200 and 100 K in the Jovian and Earth atmospheres and the (ν_4,ν_2) region is often used for remote sensing from emission measurements. They will be the subject of future works.

ACKNOWLEDGMENTS

The authors from LPPM are grateful to A. Pine for a preprint of Ref. 5 prior to publication and to D. C. Benner for the communication of some unpublished line broadening and shifting values. The LPPM and LPMA acknowledge financial support from the 1998 Program National de Chimie Atmosphérique. The work done at IEM was supported by the Spanish DGICYT under Project No. PB94-0108. The LPUB acknowledges support from the Région Bourgogne for computer equipment. M. V. Tonkov and I. M. Grigoriev were supported by the Russian Foundation for Basic research in the framework of Project No. 98-03-33105a.

APPENDIX A: LINE BROADENING AND SHIFTING DATA USED FOR ν_3 BAND LINES

As discussed in Appendix B, the model parameters $A(X,Y)$ and the quality of results are highly sensitive to the line broadening parameters used. It is thus of crucial importance to use data of the best quality possible. Unfortunately, as was shown in PPI, the values gathered in the HITRAN database for high J lines do not originate from measurements but have been ''extrapolated'' and are highly questionable. Furthermore, many previously measured values are questionable since[3] they were derived from experimental spectra with models disregarding line mixing. The line broadening and shifting data sets that we have used were thus built by us, as well as possible, as described below.

1. CH_4–Ar collisions

The line broadening data that we have used for CH_4–Ar at room temperature were built in three different steps: (i) a first set, including some of the P, Q, and R lines was directly obtained from the measured values of Ref. 2 and 13. This set remains too restricted and, for instance, does not contain any P and R lines with $J>10$. (ii) In a second step, complementary values (particularly for high J P lines) were then obtained from N_2 broadening parameters recently retrieved from experimental spectra by Benner[30] *et al.* using fits including line mixing.[3] Conversion from N_2 to Ar broadening was made by multiplying these values by the factor 0.878 as justified by the results of Refs. 2 and 13. (iii) Finally, parameters for missing lines, among which are the R transitions of high J, have been computed using the model of Ref. 16 and multiplied by a corrective factor; the latter was determined from the comparison of measured and computed results for the lines whose broadening values have been determined by steps (i) and (ii). Note that the set originating from theoretical calculations [step (iii)] is the less accurate since semiclassical models become questionable for high rotational quantum number lines.

A similar procedure was used for the determination of line shifts: (i) Refs. 2 and 13 provided a first set for CH_4–Ar. (ii) Complementary values where then obtained from CH_4–N_2 data multiplied by a factor 1.2 as roughly shown by available measurements.[2,13] (iii) Finally, values for (high J) missing lines where set to the constant value -0.006 cm^{-1}/atm.[13]

2. CH_4–He collisions

The values for He broadening of methane lines were obtained in two steps. (i) The first set, for all needed lines, was computed from the interaction potential as described in Ref. 17. (ii) These values were then corrected through the multiplication by the empirical m dependent factor deduced from comparisons[17] between computed and measured data[31] in the ν_4 band. Comparison of the resulting set with measured data for Q lines of the ν_3 band[13] has validated this procedure.

The only significant study of CH_4–He line shifts in the ν_3 band is, to our knowledge, that of Pine.[13] The measured

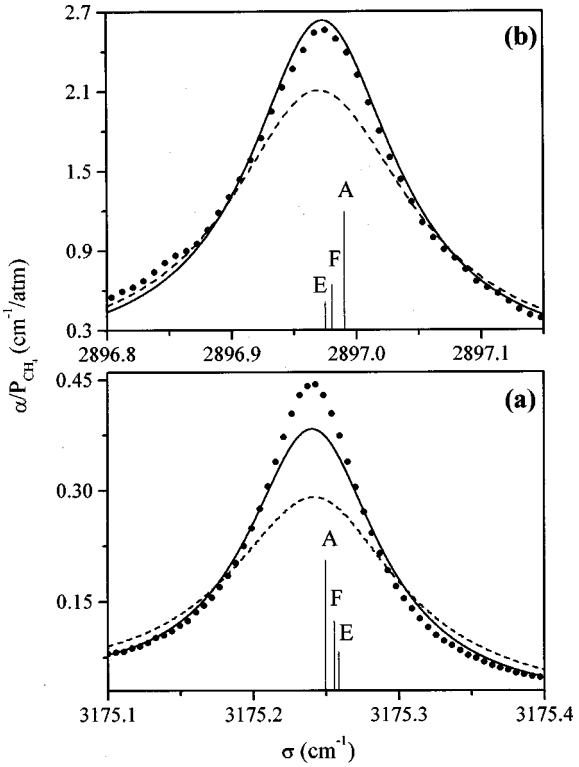

FIG. 17. Measured and calculated absorption in the *A,E,F* cluster on the high frequency side of some manifolds for CH_4–He at 1.99 atm. (a) $R(16)$ manifold (group G3); (b) $P(12)$ manifold (group G2). ● are experimental results whereas — and --- have been calculated with our line broadening database and with values from the HITRAN (Ref. 12) air-broadened values (multiplied by 0.890) (Ref. 13).

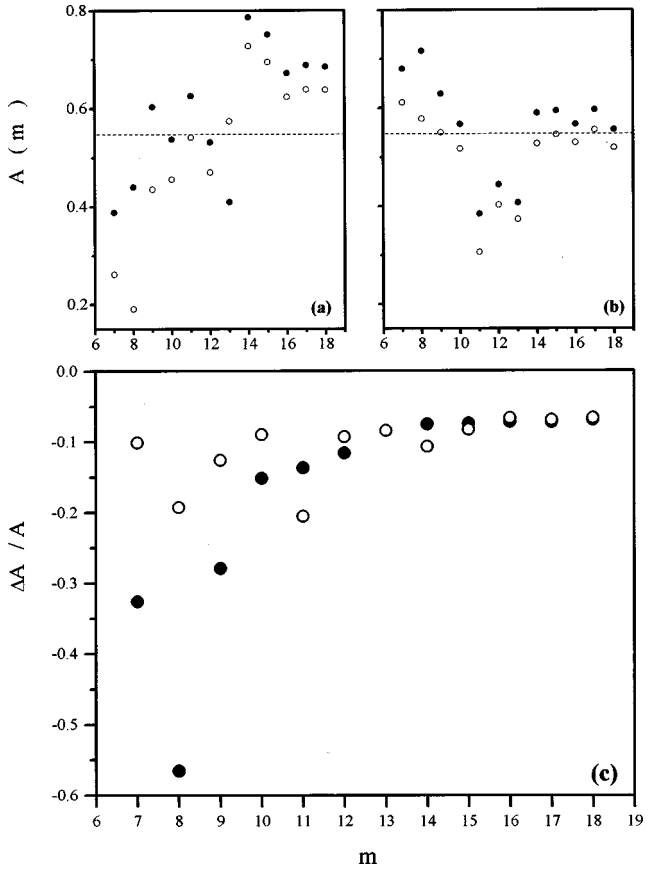

FIG. 18. $A(R_J,R_J)$ constants for CH_4–Ar in the $R6-R17$ manifolds. ● and ○ have been obtained using our line broadening data and widths lowered by 5%, respectively. The results in (a) and (b) have been obtained by medium and low pressure spectra, respectively. The plots in (c) give the relative variations of *A* introduced by the 5% change in widths when low (○) and medium (●) pressure spectra are used.

values are small and have little influence on our measured spectra. We have thus retained a constant value of $+0.001$ cm^{-1}/atm as indicated by Ref. 13.

An example of the improvement brought by our database when compared with the HITRAN[12] parameters is shown in Fig. 17 where uncoupled *A,E,F* clusters are presented. As noticed in PPI, the HITRAN values are strongly overestimated for large *J* lines. Note that for the $P(12)$ line in Fig. 17, our widths originate from the very precise N_2 broadening values by Benner,[30] and lead to very satisfactory predictions. The results for R_{16} are less satisfactory, partly due to the breakdown of the semiclassical model used to compute the corresponding widths; discrepancies may also result from the poor quality of the potential surface used[14] since much better results are obtained for CH_4–He whose interaction potential is better known.[15]

The results in Fig. 17 which are similar to what is obtained for N_2 broadening show that there is a crucial need for the improvement of line broadening values in HITRAN. Of course, for high *J R* lines, which are very closely spaced, experimental studies are difficult and a hybrid approach (including use of theoretical values) such as that used here is likely required. Furthermore, recall that the works of Benner[3] and Pine[2,13] have evidenced that a number of effects, among which is line mixing, must be accounted for while determining line widths from measured spectra.

APPENDIX B: SENSITIVITY TO BROADENING PARAMETERS

Contrary to what is done in Refs. 3, 2, 5 the line broadening and shifting parameters are input and fixed data in our approach and are not fitted together with line mixing constants. We demonstrate here that the quality of the values used have crucial influence on any conclusion concerning the modeling of line mixing with our approach. In order to do this, we have determined two sets of $A(R_J,R_J)$ constants [see Eq. (3) and Sec. III B] for the $R8-R16$ manifolds. The first was obtained using line broadening values from our database (see Appendix A) and the second by using widths 5% smaller. The values extracted from low and medium pressure spectra are compared in Fig. 18 and call for the following remarks.

The first is that uncertainties on line widths have drastic consequences on the line coupling parameters (Figs. 17 and 18). For instance, a 5% change in widths results in 33%, 14%, and 7% changes in *A* for the $R6$, $R10$, and $R14$ lines when medium pressure spectra are considered. As expected, effects are more pronounced for manifolds (low *J*) within which line coupling is small. This may explain the fact that the *J* dependence in Fig. 1 is not smooth; indeed, it would be quite easy to make $A(R_J,R_J)$ vary ''nicely'' with *J* by in-

troducing slight, *ad hoc* and line dependent, changes in the half-widths used. Note that this statement is confirmed by the results of Ref. 5.

The second is that differences between values extracted from low and medium pressure absorption may be explained by the same reason since the $A(R_J,R_J)$ parameters are then sensitive to different sets of broadening data and show different sensitivities to the widths (Fig. 18, e.g., the changes in A introduce by a 5% lowering of widths for the $R6$ lines are 33 and 10% when medium and low pressure spectra are considered). In order to prove this, take the manifolds in Fig. 3 as example. In these cases, the values of $A(R_J,R_J)$ are determined from the shape of the clusters of the low frequency side only since those on the right involve uncoupled (A,E,F) lines. The parameters retrieved from the fit are thus sensitive to the widths of the low frequency lines only. At medium pressures, all lines merge into a unique feature as shown in Fig. 5. The value of $A(R_J,R_J)$ then depends on the broadening of all lines within the manifold. Hence, inconsistencies in the half-widths may be responsible for differences between low and medium pressure results in Fig. 1. In fact, again, it would be quite easy to make these results identical by introducing slight and *ad hoc* changes in the half-widths used.

The preceding analysis demonstrates that inconsistencies of the model are due, in part, to the use of improper half-widths. Of course, errors are also likely resulting from the starting approximations of our approach that are the use of state-to-state rates, their prediction with a semiclassical approach, and the approximate nature of the interaction potential surfaces.

[1] D. C. Benner, C. P. Rinsland, V. M. Devi, M. A. H. Smith, and D. Atkins, J. Quant. Spectrosc. Radiat. Transf. **53**, 705 (1995).
[2] A. S. Pine, J. Quant. Spectrosc. Radiat. Transf. **57**, 145 (1997).
[3] V. M. Devi, D. C. Benner, M. A. H. Smith, C. P. Rinsland, G. Guelachvili, and L. R. Brown, 53rd Int. Symp. on Mol. Spectrosc, Paper WF10-WF12, Columbus, OH, 1998.
[4] D. Pieroni, Nguyen-Van-Thanh, C. Brodbeck, C. Claveau, A. Valentin, J.-M. Hartmann, T. Gabard, J.-P. Champion, D. Bermejo, and J.-L. Domenech, J. Chem. Phys. **110**, 7717 (1999).
[5] A. S. Pine and T. Gabard, J. Quant. Spectrosc. Radiat. Transf. (in press).
[6] T. Gabard and J.-P. Champion, J. Quant. Spectrosc. Radiat. Transf. **52**, 303 (1994).
[7] D. V. Kalinin, D. K. Bronnikov, Yu. G. Selivanov, T. Gabard, J.-P. Champion, and J.-C. Hilico, J. Quant. Spectrosc. Radiat. Transf. **62**, 13 (1999).
[8] Q. Ma, R. H. Tipping, G. Birnbaum, and C. Boulet, J. Quant. Spectrosc. Radiat. Transf. **59**, 259 (1998).
[9] R. Rodrigues, B. Khalil, R. Le Doucen, L. Bonamy, and J. M. Hartmann, J. Chem. Phys. **107**, 4118 (1997).
[10] S. Angus, B. Armstrong, and K. M. de Reuck, *International Thermodynamic Tables of the Fluid State: Argon* (Pergamon, Oxford, 1971).
[11] S. Angus and K. M. de Reuck, *International Thermodynamic Tables of the Fluid State: Helium-4* (Pergamon, Oxford, 1977).
[12] L. S. Rothman, (HAWKS 1996) the HITRAN atmospheric workstation, ASA meeting, Reims, France, 4–6 Sept. (1996).
[13] A. S. Pine, J. Chem. Phys. **97**, 773 (1992).
[14] U. Buck, J. Schleusener, D. J. Malik, and D. Secrest, J. Chem. Phys. **74**, 1707 (1981).
[15] U. Buck, K. H. Khol, A. Kohlhase, M. Faubel, and V. Staemmler, Mol. Phys. **55**, 1255 (1985).
[16] T. Gabard, J. Quant. Spectrosc. Radiat. Transf. **57**, 177 (1997).
[17] T. Gabard, J. Quant. Spectrosc. Radiat. Transf. **59**, 287 (1998).
[18] T. G. A. Heijmen, T. Korona, R. Moszynski, P. E. S. Worner, and A. Van Der Avoird, J. Chem. Phys. **107**, 902 (1997).
[19] M. O. Bulanin, A. B. Dokuchaev, M. V. Tonkov, and N. N. Filippov, J. Quant. Spectrosc. Radiat. Transf. **31**, 521 (1984).
[20] R. Rodrigues, C. Boulet, L. Bonamy, and J. M. Hartmann, J. Chem. Phys. **109**, 3037 (1998).
[21] J. M. Hartmann, R. Rodrigues, Nguyen-Van-Thanh, C. Brodbeck, C. Boulet, R. Le Doucen, N. Lacome, and L. Bonamy, J. Chem. Phys. **110**, 7733 (1999).
[22] J. P. Bouanich, J. M. Hartmann, Gh. Blanquet, J. Walrand, D. Bermejo, and J. L. Domenech, J. Chem. Phys. **109**, 6684 (1998).
[23] L. Ozanne, Nguyen-Van-Thanh, C. Brodbeck, J. P. Bouanich, J. M. Hartmann, and C. Boulet, J. Chem. Phys. **102**, 7306 (1995).
[24] J. M. Hartmann and F. L'Haridon, J. Chem. Phys. **103**, 6467 (1995).
[25] C. Cousin, R. Le Doucen, C. Boulet, A. Henri, and D. Robert, J. Quant. Spectrosc. Radiat. Transf. **36**, 521 (1986).
[26] J. M. Hartmann, M. Y. Perrin, Q. Ma, and R. H. Tipping, J. Quant. Spectrosc. Radiat. Transf. **49**, 675 (1993).
[27] C. Boulet and D. Robert, J. Chem. Phys. **77**, 4288 (1982).
[28] C. Boulet, J. Boissoles, and D. Robert, J. Chem. Phys. **89**, 625 (1988).
[29] J. Boissoles, V. Menoux, R. Le Doucen, C. Boulet, and D. Robert, J. Chem. Phys. **91**, 2163 (1989).
[30] D. C. Benner (private communication): widths and shifts of line in the ν_3 band region retrieved from fits of multiple experimental spectra.
[31] J. S. Margolis, J. Quant. Spectrosc. Radiat. Transf. **55**, 823 (1996).